International Journal of Science and Engineering Applications
Volume 6–Issue 12, 350-359, 2017, ISSN:-2319–7560

Evaluating Security-as-a-Service (SECaaS) Measures to Increase the Quality of Cloud Computing

Khaled M. Musa

Sullivan University
Louisville, Kentucky, USA

Abstract: Cloud computing is the new theme of information technology. There are companies, agencies, and individual users that have adopted cloud computing at their work, and others are still considering adopting the new technology. The cloud environment is a virtual environment that offers services to various clients based on their need of service. Cloud computing offers services such as infrastructure (IaaS), platform services (PaaS), and software (SaaS). The providers of cloud computing services found that security measures are extremely needed to protect data and resources used by clients. Security-as-a service (SECaaS) is a new service implemented in the cloud computing environment to protect the IaaS, PaaS, and SaaS along with all data and resources that are used within the clouds. To provide secure environment, cloud computing providers are implementing several components of SECaaS that constitute security measures in cloud computing. IT managers and decision makers in various businesses aim to use adequate new technology to protect business data and resources. SECaaS in its various security services is a new technology for businesses to adopt for the protection of their data and resources. This research will evaluate identity and access management, data loss prevention, encryption capabilities, vulnerability management, and email security SECaaS measures and controls that would increase the quality of cloud computing. In this paper, there will be an evaluation to some of the common used SECaaS measures such as identity and access management, data loss prevention, encryption capabilities, vulnerability management, and email security on their importance to be key factors in the standardization of SECaaS measures of cloud computing.

Keywords: Cloud Environment, Cloud Computing, Software-as-a-service (SaaS), Platform-as-a-service (PaaS), Infrastructure-as-a-service (IaaS), Security as-a-service (SECaaS), Security Standards.

1. INTRODUCTION

Innovations in server centric computing have led to improved Internet-based structures called cloud computing (Mell & Grance, 2011). According to Mell & Grance (2011), cloud computing is described as Internet-based services accessed by different users, as shown in Figure 1. Cloud computing gives accessible visualized services such as software, storage, and programming capabilities from anywhere over the internet (Hussain & Abdulsalam, 2011), the cloud environment in its services allows organizations to avoid high investments in new computer networks, hardware, software and software licensing (Ardagna, Asal, Damiani, & Vu, 2015).

In this paper, there will be analyzation to how SECaaS specific measures of cloud computing would influence the adoption of cloud computing. It seeks to help cloud computing providers place emphasis on the implementation of stronger SECaaS measures and further standardizing SECaaS measures.

The results of this study are expected to provide information on key SECaaS measures, and their impact and significance to be included in SECaaS standardized measures offered by quality control bodies of cloud computing. In investigating the measures of SECaaS will yield information related to what measures implemented in SECaaS can be standardized for cloud providers to follow to provide safer and risk-free cloud environment.

The rest of this paper is organized as follows: section 2 presents an overview of the types of cloud computing services. Section 3 discusses the Security -as-a-Service (SECaaS) measures. Section 4 Evaluating SECaaS measures and controls. Finally, section 5 concludes the paper.

2. TYPES OF SOFTWARE TESTING

Although there are many cloud computing services, this paper will only include the following main services:

- **Software-as-a-service (SaaS):** a cloud computing model that provides software applications to be used by various clients via internet (Hussain & Abdulsalam, 2011).

- **Platform-as-a-service (PaaS):** a cloud computing model that provides users the ability to develop, customize and manage software applications (Hussain & Abdulsalam, 2011).

- **Infrastructure-as-a-service (IaaS):** a cloud computing model that provides clients top access, monitor, and manage their remote infrastructures such as storage, networks, and network services (Hussain & Abdulsalam, 2011).

- **Security-as-a-service (SECaaS):** a cloud computing model that provides IT security measures to protect information and software from any fraudulent and intruding issues (Hussain & Abdulsalam, 2011).

- **Security-as-a-Service (SECaaS) Measures**

SECaaS measures vary between simple antivirus measures to having large servers with firewalls to protect all attributes of the business that are important to various agencies, businesses, and persons. Tirado (2008) sought that security engineers should focus on the SECaaS measures that contribute to the failures or success of business processes and goals.
Integrating SECaaS measures and controls allow cloud computing to enforce common security measures to protect information and software systems in the cloud environment (Reddy & Kaylan, 2014).

Chow, Golle, Jakobsson, Shi, Staddon, Masuoka, & Molina, (2009) examined the SECaaS measures that prevented companies from adopting cloud computing, but the security measures addressed in the study were based on the references of World Privacy Forum Report and Information Security magazine.

To increase the reliability of this research, this research will use the SECaaS measures and controls that match IT security standards that are shared between Cloud Security Alliance (CSA) organization, Cloud Standards Customer Council (CSCC), Open Data Center Alliance (ODCA), and National Institute of Standards and Technology (NIST).

The SECaaS security standards constituted by the common bodies of cloud computing standardization are identity and access management, data loss prevention, web security, email security, intrusion management, encryption capabilities, disaster recovery, network security, and vulnerability management. All these factors are equally important.

Looking at the different bodies that standardize the various cloud computing SECaaS measures, this research seeks to examine the common SECaaS measures the include the following measures:

- **The Identity and Access Management** component of SECaaS manages people, processes, and systems. The identity and access man-

agement ensure security as part of the cloud computing environment where it verifies identity, grant access levels to users to services and information (CSA, 2015).

- **Data Loss Prevention** or data loss protection describes the controls in SECaaS that ensure data resides for specific authorized users (CSA, 2015)

- **Information Encryption/ Decryption** capabilities is a SECaaS component that uses cryptography to protect data by providing encryption and decryption keys granted to authorized users to access their data only when needed (CSA, 2015).

- **Vulnerability Management** is a component of SECaaS that continually monitor the cloud computing components for deviation from enforced controls and standardize all inputs and outputs to enhance interoperability (Aros, n.d.).

- **Email Security** is a component of SECaaS to ensure security by monitoring and mitigating threats such as spam, phishing, malware propagation using emails. The email security component inspects, filter, and protect data using decryptions and digital signature (CSA, 2015)

3. EVALUATING SECAAS MEASURES AND CONTROLS

Evaluating the SECaaS measures using the IBM Statistical Package for Social Science (SPSS) statistics Version 22.0 software was performed using the on the completed survey responses. Using SPSS, descriptive analysis was calculated using numerical values of Likert scale where values range between 1 which is strongly disagree to 5 strongly agree. The resulting SPSS analysis of variance (ANOVA), on the 109-population sample, compared the values for each dependent variable with the values for the dependent variable. The descriptive statistics for the different variables addressed in the original responses of the survey are listed in the below table 1.

	N	Range	Mini-mum	Maxi-mum	Sum	Mean	Mean	Std. Devi-ation	Vari-ance
	Statistic	Statis-tic	Statistic	Statistic	Statis-tic	Statis-tic	Std. Error	Statistic	Statistic
Identity and Access Management	109	4.00	1.00	5.00	472.25	4.3326	.07488	.78178	.611
Data Loss Preven-tion	109	4.00	1.00	5.00	473.25	4.3417	.07335	.76578	.586
Information En-cryption/ Decryp-tion	109	4.00	1.00	5.00	465.75	4.2729	.07173	.74887	.561
Vulnerability Man-agement	109	4.00	1.00	5.00	466.50	4.2798	.07900	.82476	.680
Email Security	109	4.00	1.00	5.00	455.00	4.1743	.09150	.95531	.913
Valid N (listwise)	109								

Table 1. Descriptive Statistics Original Data.

In the descriptive statistics original data, there are five independent variables: identity and access management, data loss prevention, information encryption/decryption, vulnerability management, and email security. The descriptive statistical analysis table that contains the five variables show the range of values are between minimum 1 and maximum 5, and the mean which is the average of all values is between 4.17 to 4.34.

Each question addresses it's influence on the decision to adopt cloud computing. Each of all five dependent variables seem to have a mean that is greater than 4 which is the value of "Agree" to the importance of the variable to include in standardization requirements.to cloud computing. All variables are equally important on the decision to adopt cloud computing. The mean of every variable differs from another and the closer the values to the maximum value of 5, the more participants agree that it should be important to standardization of SECaaS measures of cloud computing.

The standard deviation measures the average distance from the mean or the dispersion of set of data from the mean (Burns & Burns, 2013) which found to be from .748 to .955. The variance measures how far data is spread, and its values are between .561 to .931.

Examining the standard deviation of the five independent variables, the four variables identity and access management, data loss prevention, information encryption/decryption, vulnerability management, seem to have relatively close variations from their mean with values between .749 and .824; whereas the variable email security seem to have larger deviation value of .955 from the mean. The closer the standard deviation to zero, the closer data points to the mean. None of the variables have a value that is close to zero, but all relatively close to each other's. The variable Email security, seem to have larger standard deviation or variance from each other.

The five independent variables identity and access management, data loss prevention, information encryption/decryption, vulnerability management, and email security vary in their influences to adopt cloud computing. Analyzing the five variables to distinguish the

difference in the influence the decision to adopt cloud computing, "Agree" will represent the "Strongly Agree or "Agree" responses whereas "Disagree" will represent "Strongly Disagree" or "Disagree".

4. EVALUATING IDENTITY AND ACCESS MANAGEMENT

Analyzing the identity and access management variable, we find that out of the 109 participants 89 agree which is a representation to strongly agree or agree, that the variable will influence the decision to include it in the standardization of SECaaS measures whereas 20 disagrees which is a representation to strongly disagree or disagree, that the variable influences to include it in the standardization of SECaaS measures, Figure 1.

Further, analyzing the identity and access management variable using the p-value (P) to determine the significance of the identity and access management variable. In table 2, the Significance is greater than .0005 ($P < .0005$) which means that the identity and access management is statistically significant element as SECaaS measures.

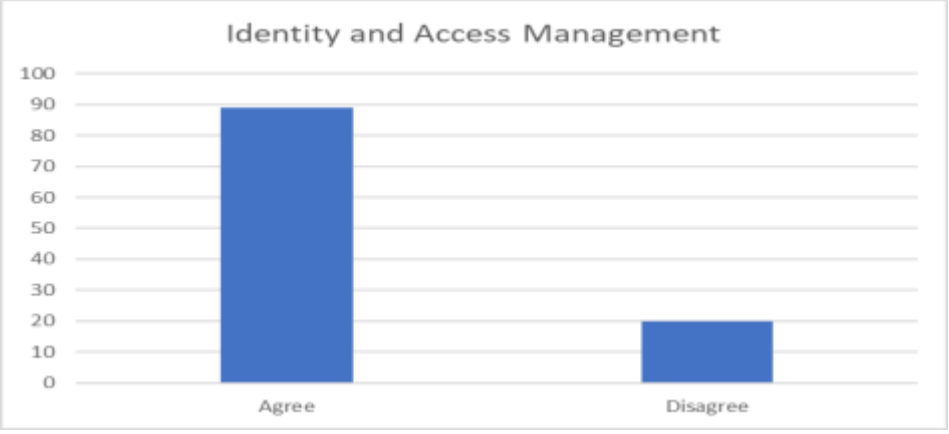

Figure 1. Identity and Access Management

ANOVA[a]

Model		Sum of Squares	Df	Mean Square	F	Sig.
1	Regression	42.340	1	42.340	409.046	.000[b]
	Residual	11.075	107	.104		
	Total	53.415	108			

Table 2. Identity and Access Management ANOVA Analysis

5. EVALUATING DATA LOSS PREVENTION

Analyzing the data loss prevention variable, we find that out of the 109 participants 91 agree, represent strongly agree or agree, that the variable will influence the decision to adopt cloud computing whereas 18 disagrees, represent strongly disagree or disagree, that the variable influences to include it in the standardization of SECaaS measures, Figure 2. Further, analyzing the data loss prevention variable using the p-value (P) to determine the significance of the data loss prevention variable.

Figure 2: Data Loss Prevention

ANOVA[a]

Model		Sum of Squares	df	Mean Square	F	Sig.
1	Regression	41.145	1	41.145	358.802	.000[b]
	Residual	12.270	107	.115		
	Total	53.415	108			

Table 3. Data Loss Prevention ANOVA Analysis

6. EVALUATING INFORMATION ENCRYPTION/ DECRYPTION

Analyzing the information encryption/ decryption variable, we find that out of the 109 participants 91 agree, represent strongly agree or agree, that the variable will influence the decision to adopt cloud computing whereas 18 disagrees, represent strongly disagree or disagree, that the variable influences to include it in the standardization of SECaaS measures, Figure 3.

In table 3, the Significance is greater than .0005 (P < .0005) which means that data loss prevention is statistically significant element as SECaaS measures

Further, analyzing the identity and access management variable using the p-value (P) to determine the significance of the information encryption/ decryption variable. In table 3, the Significance is greater than .0005 (P < .0005) which means that the information encryption/ decryption is statistically significant element as SECaaS measures.

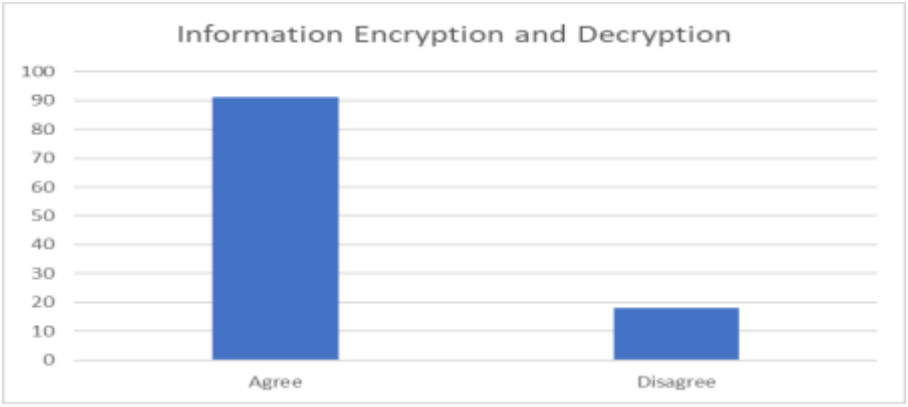

Figure 3. Information Encryption/ Decryption

ANOVA[a]

Model		Sum of Squares	df	Mean Square	F	Sig.
1	Regression	38.996	1	38.996	289.377	.000[b]
	Residual	14.419	107	.135		
	Total	53.415	108			

Figure 1. Identity and Access Management

7. EVALUATING VULNERABILITY MANAGEMENT

Analyzing the vulnerability management variable, we find that out of the 109 participants 103 agree, represent strongly agree or agree, that the variable will influence the decision to adopt cloud computing whereas 6 disagrees, represent strongly disagree or disagree, that the variable influences to include it in the standardization of SECaaS measures, Figure 4.

Further, analyzing the vulnerability management variable using the p-value (P) to determine the significance of the information encryption/ decryption variable.

In table 5, the Significance is greater than .0005 (P < .0005) which means that the vulnerability management is statistically significant element as SECaaS measures.

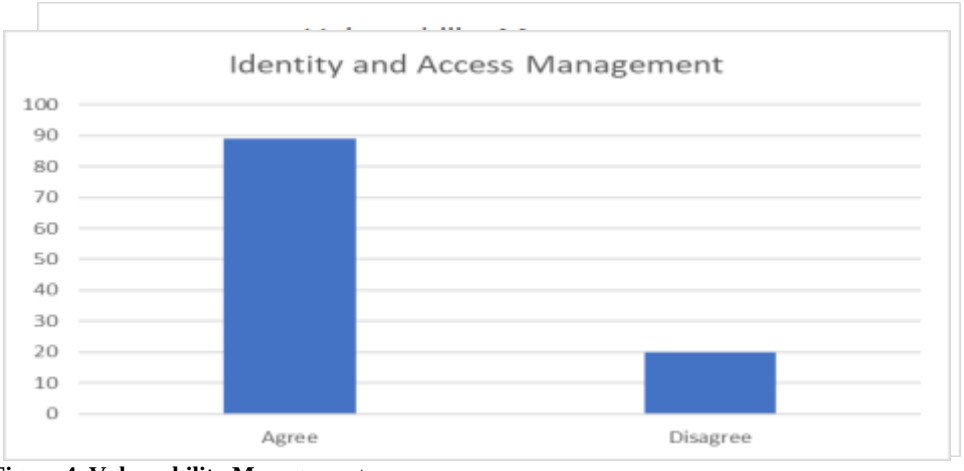

Figure 4. Vulnerability Management

ANOVA[a]

Model		Sum of Squares	df	Mean Square	F	Sig.
1	Regression	42.214	1	42.214	403.255	.000[b]
	Residual	11.201	107	.105		
	Total	53.415	108			

Table 5. Vulnerability Management ANOVA Analysis

8. EVALUATING EMAIL SECURITY

Analyzing the email security variable, we find that out of the 109 participants 87 agree, represent strongly agree or agree, that the variable will influence the decision to adopt cloud computing whereas 22 disagrees, represent strongly disagree or disagree, that the variable influences the decision to include it in the standardization of SECaaS measures, Figure 5.

Further, analyzing the email security variable using the p-value (P) to determine the significance of the information encryption/ decryption variable.

In table 6, the Significance is greater than .0005 (P < .0005) which means that the email security is statistically significant element as SECaaS measures.

Figure 5: Email Security

ANOVA[a]

Model		Sum of Squares	df	Mean Square	F	Sig.
1	Regression	35.168	1	35.168	206.219	.000[b]
	Residual	18.247	107	.171		
	Total	53.415	108			

Table 6. Email Security ANOVA Analysis

4. CONCLUSION

The common five SECaaS measures that include identity and access management, data loss prevention, information encryption/ decryption, vulnerability management, and email security. The 109 participants agreed on the importance that all five SECaaS measures which signify the purpose to include them in standardizing SECaaS. The ANOVA analysis for each measure indicated the high significance of each variable to SECaaS standards. The analysis of all variables shows close results to their importance to cloud computing, despite the different readings they give. Many of all participants agreed that data loss prevention and information encryption/ decryption have the highest votes to its importance, following identity and access management, following email security.

REFERENCES

[1] D. Galin, Software Quality Assurance: From Theory to Implementation, Addison Wesley, New York, NY, USA, 2003.

[2] ISO, ISO/IEC TR 19759: Guide to the Software Engineering Body of Knowledge (SWEBOK), International Organization for Standardization, Geneva, Switzerland, 2005.

[3] S. Chat, Performance Management of Software Architecture, online: http://www.findwhitepapers.com/whitepaper2373/, visited on July 4, 2009.

[4] G. J. Myers, T. Badgett, T. M. Thomas, and C Sandler, the Art of Software Testing, Wiley, USA, 2004.

[5] ApTest, Web QA Test Tool Links, online: http://www.aptest.com/webresources.html, visited on April 15, 2009.

[6] INSECURE, Top 100 Network Security Tools online: http://sectools.org/, visited on April 20, 2009.

[7] Java-Source, Open Source Testing Tools in Java, online: http://java-source.net/open-source/testing-tools, visited on April 20, 2009.

[8] Ranorex, Web Testing, online: http://www.ranorex.com/support/user-guide-20/web-testing.html, visited on April 22, 2009.

[9] Bright-Hub, Sniffing Data with Ettercap for Linux and Windows, online: http://www.brighthub.com/computing/smb-security/articles/35545.aspx, visited on April 22, 2009.

[10] QFS, Facts & Features, online: http://www.qfs.de/en/qftest/, visited on April 23, 2009.

International Journal of Science and Engineering Applications
Volume 6–Issue 12, 364-371, 2017, ISSN:-2319–7560

Design and Performance Evaluation of an Air-Blast Atomizer

Dr. Olusegun Adefonabi Adefuye
Department of Mechanical Engineering,
Lagos State University,
Lagos, Nigeria

Benneth Ifenna Okoli
Centre for Space Transport and Propulsion,
National Space Research and Development Agency,
Abuja, Nigeria

Abstract: The present work describes the design, construction and experimental investigations of an air-blast atomizer for half spray cone angle of 30° using stainless steel for foundry application. Outline detail of experimental setup to investigate effect of injection pressures on spray and flame lengths, the amount of fuel and the time taken to melt some selected materials was studied. An experimental study of air-blast atomization was conducted using the manufactured atomizer in which the fuel (kerosene) flows under gravity at angle 45^{o} from the tank and was atomized by the oxygen stream flowing in a cylindrical channel from a pressurized oxygen bottle (cylinder). Produced air-blast atomizer was experimentally investigated at different pressures ranging from 3 to 15 bars in the step of 3 bars [6].

As the injection pressure was increased from 3 to 15 bars, the spray and flame lengths increases. From 6 to 12 bars, visible increment was observed in the spray and flame lengths due to increase in injected pressure which led to breaking-up of the liquid film into small droplets. As enough pressure was provided from 12 to 15 bars, spray and flame lengths increased appreciably. 0.6 kg of aluminum melted in 13 minutes 43 seconds using 0.5 liter of kerosene; the volumetric flow rate and the mass flow rate obtained was $6.075*10^{-7}$ m^3/sec and $4.921*10^{-4}$ kg/sec respectively. Similarly, 1.2 kg of brass melted in 17 minutes 13 seconds using 1 liter of kerosene; the volumetric flow rate and the mass flow rate obtained was $9.680*10^{-7}$ m^3/sec and $7.841*10^{-4}$ kg/sec respectively. The furnace efficiency of 2.2 % was calculated from the theoretical and actual energy used for melting the metal [6].

Keywords: Air-blast atomizer; stainless steel; kerosene; spray cone angle; furnace; foundry.

1. INTRODUCTION

Atomization is a process whereby a volume of liquid is converted into a multiplicity of small drops [1]. Its principal aim is to produce a high ratio of surface to mass in the liquid phase, resulting in very high evaporation rates. Air-blast atomizers have many advantages over pressure atomizers, especially in their application to gas turbine engines of high pressure ratio. They require lower fuel pressures and produce a finer spray. Moreover, because the air-blast atomization process ensures thorough mixing of air and fuel, the ensuing combustion process is characterized by very low soot formation and a blue flame of low luminosity, resulting in relatively cool liner walls and a low exhaust smoke. The merits of the air-blast atomizer have led in recent years to its installation in a wide range of industrial and aircraft engines. Most of the systems now in service are of the "pre-filming" type, in which the fuel is first spread out into a thin, continuous sheet and then subjected to the atomizing action of high velocity air. In other designs, the fuel is injected into the high-velocity airstream in the form of one or more discrete jest. In all cases the basic objective is the same, namely, to deploy the available air in the most effective manner to achieve the best possible level of atomization [1].

Madu [2] designed, constructed and tested a burner that uses an admixture of used engine oil and kerosene for foundry application. Tests were carried out to determine the time taken to melt 1 kg each of the selected engineering materials (copper, aluminum, brass, and lead). It took 49 minutes, 15 minutes, 22 minutes, and 7 minutes to melt copper, aluminum, brass, and lead respectively.

Robert [3] studied the effect of atomization gas properties on droplet atomization in an air-assist atomizer where air and fuel mix within the nozzle before exiting through the outlet orifice. He used air, nitrogen, argon, and carbon dioxide as the atomizing gas to determine the effect of each of these gases on mean droplet size, number density, velocity and their distributions in kerosene fuel sprays. Data were obtained with these atomizing gases using a base, air assisted case as a reference. Comparisons were made between the gases on a mass and momentum flux basis. The results show that the presence of oxygen in the air atomized sprays assists in the combustion process, since it produces smaller and faster moving droplets, especially at locations near to the nozzle exit. Lighter gases such as nitrogen more effectively atomized the fuel in comparison to the denser gases. Argon and carbon dioxide produced larger, slower moving droplets than air and nitrogen assisted cases.

Witold [10] studied kerosene atomization process under high speed air stream. Experiments showed that in the case of stream-type injectors (atomizers), a large number of small injection holes in detonation chamber should be applied in relation to disintegration of injected fuel as well as spatial uniformity of created combustible mixture.

Pipatpong [11] developed an air-assisted fuel atomizer for a continuous combustor. They summarized that low pressure air atomization of refine palm oil fuel with air pressure in the range of 69 – 620 kPa can be used to develop air blaster or burners.

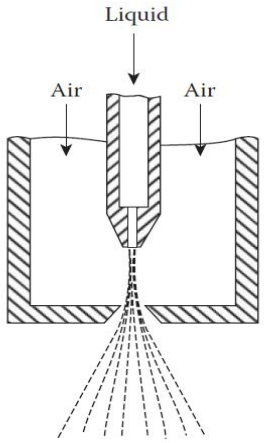

Figure 1: Schematic of an air-blast atomizer [4].

2. MATERIALS AND METHODOLOGY

2.1 Materials selection

The selection of materials to be used for the different components in this design involves the following consideration:

i. Cost and availability of the material.
ii. Material property – mechanical, physical and chemical properties (that is, its ability to resist corrosion due to prolonged usage).

2.2 Properties of fuel used

The kerosene fuel sample was collected from Nigerian National Petroleum Corporation (NNPC) approved gas station in Lagos – Nigeria. The specification of the fuel is presented below.

Table 1: Properties of fuel used [5].

Property	Unit	Kerosene
Chemical formula	-	$C_{10}H_{22}$
Calorific value	kJ/kg	45400
Self-ignition temperature	^oC	640
Final boiling point	^oC	249
Ignition delay period	S	0.0015
Flame propagation rate	cm/s	11.8
Flame temperature	^oC	1782
Kinematic viscosity @ 39^oC	m^2/s	2.2
Specific gravity @ 15.6/15.6 ^oC	-	0.843
Colour	-	Colourless
Sulphur content	wt %	0.04

Table 2: Other materials used and their properties

S/N	Parts	Material Selected	Material Property
1	Fuel tank	Mild steel	Strength and ability to resist corrosion.
2	Hose	i. Galvanized ii. Polymer	i. Ability to resist corrosion. ii. Chemically inert to oil.
3	Fuel stand	Mild steel	Strength and ability to resist corrosion.

2.3 Design considerations for the atomizer

The air passage should be made aerodynamically smooth, with minimum areas at the atomization edge to obtain maximum air velocities and to maintain them during initial disintegration process. The cylindrical part of the injector nozzle should be short; an increase of nozzle length is undesirable, since it leads to a decrease of the root angle of the spray. It is recommended that the cone angle on the horizontal entrance be within limits from 60^0 to 120^0 [7]. It is advisable to calculate these parameters on the basis of the theory of the spray, using the curves shown below:

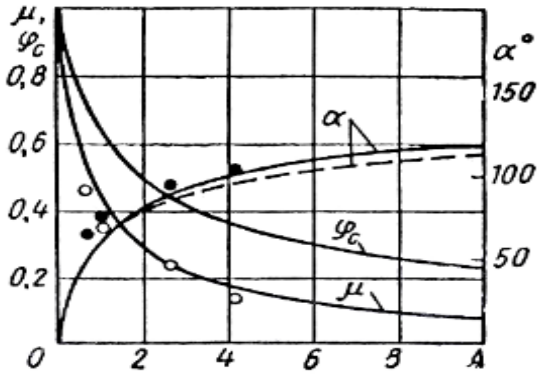

Figure 2: Dependence of discharge coefficient μ, nozzle space factor ϕ and spray angle ∝ on the geometric characteristic of the injector A - experimental points [7].

Determining the dimension of the air-blast atomizer from Figure 2; the spray angle α was chosen to be 60^0. Diameter of the nozzle orifice, d_c was calculated using equations 1 and 2 below:

$$d_c = \sqrt{\frac{4G}{\pi C_d \sqrt{2\rho\Delta P}}} \quad (1)$$

Where:

G = mass flow rate

C_d = 0.27 = discharge coefficient (from Figure 2)

ρ = 810 kg/m^3 = density of kerosene

P_1 = 3 bars = 300,000 Pa = injected pressure

$P_{atm.}$ = 101,300 Pa = atmospheric pressure

$\Delta P = P_1 - P_{atm.}$ = 198,700 Pa = pressure differential

But,

$$G = \rho Q = C_d A\sqrt{2\rho\Delta P} \quad (2)$$

The effect of viscosity on the atomizer (nozzle) is given by the Reynolds number at the inlet of the atomizer:

$$\mathrm{Re} = \frac{4G}{\pi\rho\vartheta\sqrt{id}_c} \quad (3)$$

Where:

ϑ the contraction coefficient (assumed from the range of 0.85 - 0.90) [9]. d_c is the diameter of the nozzle. After calculation of d_c, other geometrical sizes of the injector: the nozzle length l_c, length of entrance port $l_{oz,}$ diameter of inlet port d_{oz}, was selected based on [8] approach.

Table 3: Design parameters for the air-blast atomizer

Design Data	Nozzle half spray angle 30^0
Diameter of nozzle, d_c	0.89 mm
Number of inlet ports, n	2
Diameter of inlet port, d_{oz}	3 mm
Length of entrance port, l_{oz}	40 mm
Nozzle Length, l_c	50 mm

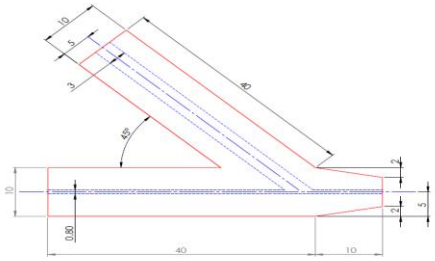

Figure 3: Manufacturing diagram of the atomizer [6].

2.4 Flow of kerosene from the fuel tank to the atomizer

Using the energy conservation concept to determine the velocity of flow along a pipe from a reservoir, we considered the ideal reservoir in Figure 4 below.

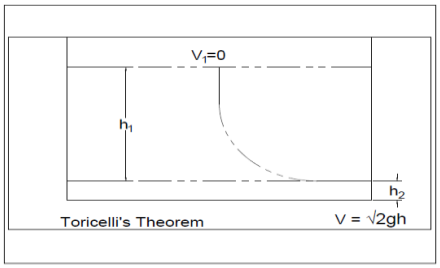

Figure 4: An ideal reservoir.

The level of the fuel in the reservoir is h_1. Considering the energy situation – there is no movement of the fuel, so kinetic energy is zero but the gravitational energy is:

$$mgh \quad (4)$$

If the pipe is attached at the bottom, fuel flows along this pipe out of the tank to a level h_2. A mass, m has flowed from the top of the reservoir to the nozzle and it has gained a velocity, v.
So, from Torricelli's equation:

$$v = \sqrt{2g(h_1 - h_2)} \quad (5)$$

We now have an expression for the velocity of the fuel as it flows from the fuel tank to the atomizer at a height ($h_1 - h_2$) below the surface of the reservoir.

Where:
h_1 = 2.1 m = height of fuel tank stand + height of fuel level in the tank
h_2 = 0 = height of atomizer (ground level)
g = 9.81 m/s^2 = acceleration due to gravity
ρ = 810 kg/m^3 = density of kerosene

Fuel velocity, v

$$v = \sqrt{2g(h_1 - h_2)} \quad (6)$$

$$v = \sqrt{2 * 9.81 * 2.1} = 6.42 \text{ m/s}$$

Pressure inside the fuel pipe, P

$$P = \rho gh \quad (7)$$

$$= 810 * 9.81 * 2.1 = 16686.81 \text{ Pa}$$

2.5 Separation losses in pipe flow

These are losses which occur as a result of various pipes fittings such as bends, valves, and also sudden enlargement and contraction of the pipe. For losses due to friction, using Darcy -Weisbach equation:

$$h_f = f\frac{l}{d}\frac{v^2}{2g} \quad (8)$$

But, Reynolds number for a pipe is given by:

$$\mathrm{Re} = \frac{\rho v d_h}{u} = \frac{v d_h}{u} \quad (9)$$

Where:
v = 6.4 m/s = fuel velocity
u = kinematic viscosity (1 cst = 10^{-6} m^2/s) = 2.2 * 10^{-6} m^2/s
d_h = hydraulic diameter

$$d_h = \frac{4\left(\pi r_o^2 - \pi r_i^2\right)}{\left(2\pi r_o + 2\pi r_i\right)} = 2\left(r_o - r_i\right) \quad (10)$$

d_o = 0.0102 m = external diameter of fuel pipe, r_o = 5.1*10^{-3} m = external radius of fuel pipe.
d_i = 0.01 m = internal diameter of fuel pipe, r_i = 5*10^{-3} m = internal radius of fuel pipe.

$d_h = 2* 10^{-4}$ m and $\text{Re} = \frac{\rho v d_h}{u} = \frac{v d_h}{u}$

Where:
d_i = 0.01 m = internal diameter of fuel pipe
h_f = head loss due to friction in the pipe
f = friction coefficient
v = 6.42 m/s = fuel velocity
l = 2.97 m = length of fuel pipe

Re = 583.64 Pa

Since the flow is laminar as Reynolds number is less than 2000,

$$f = \frac{64}{\text{Re}} = 0.11$$

$$\therefore h_f = f \frac{l}{d} \frac{v^2}{2g} = 64.42 \text{ Pa}$$

2.6 Test facility

A schematic of the test facility is shown in Figure 6, the atomizer was mounted on a thick plate for support and the fuel and oxygen pipes were fixed to the adaptors. The oxygen for the test was provided from oxygen refrigerant cylinder of 150 bars pressure capacity. A pressure regulator was used to keep the pressures constant at any pressure injection feed. The different parts of the atomizer were assembled together in the following order: the oxygen inlet and fuel inlet adapter was bolted to the atomizer and finally, the fuel hose and the oxygen hose was connected to the fuel inlet and to the oxygen inlet adapter respectively. The burning device operates on the principle of combustion in which oxygen (air) is required or supplied to enhance burning [6].

2.7 Experimental investigations

The fuel (kerosene) was stored in a tank of 0.8 m length and 0.4 m diameter mild steel of 27 litres capacity, the liquid flows under gravity and injected through a small diameter orifice at the centerline of the atomizer. A calibrated valve was used to regulate the flow of kerosene from the fuel tank. Pressurized oxygen (air) was injected through a pipe to the fuel pipe and the fuel drops through the pipe duct at an angle of 45^o to form the liquid streams. The nozzle increases the velocity of the fluid [6].

The experimental setup was developed for the measurement of spray characteristics like spray lengths and flame lengths at different pressures varying from 3 to 15 bars. Photographs were taken by high speed camera to capture the spray lengths and flame lengths at different injected pressures. Also the time taken to melt the selected materials was also obtained.

2.7.1 Determination of spray lengths at different injected pressures

The rate of flow of fuel from the tank was kept constant for all the experiments by controlling the valve. The pressurized oxygen and kerosene were well mixed before exiting the atomizer. Visible atomization process was observed as the mixture of oxygen and kerosene was seen discharging through the atomizer (nozzle) orifice. Using a pressure regulator attached to the oxygen bottle; at different injected pressures ranging from 3 to 15 bars, the spray lengths were captured using a camera [6].

2.7.2 Determination of flame lengths at different injected pressures

The pressurized oxygen and kerosene were well mixed before exiting the atomizer. Visible atomization process was observed as the mixture of oxygen and kerosene was seen discharging through the atomizer (nozzle) orifice. The atomizer sprays the mixture and it was ignited using a lighter. With the help of the pressure regulator attached to the oxygen bottle; at different injected pressures ranging from 3 to 15 bars, the flame lengths were captured using a camera [6].

2.7.3 Determination of time taken to melt metal charge

The volume of kerosene in the fuel tank was noted. The crucible pot and the metal charge to be melted was prepared and weighed using digital weighing machine. The crucible pot with the metal inside was placed in a pit furnace and the taps that controls the fuel and the oxygen line was opened. Once visible atomization process was observed the fuel was ignited. As the fuel was ignited, a stop watch was used to check how long it took to melt a particular metal. Before and after each test (melting of the metals), the volume of kerosene was noted and the difference between the initial and the final volume gives the amount of kerosene used to melt the metal [6].

3. RESULTS AND DISCUSSIONS

Figure 5: Designed atomizer [6].

Figure 6: Complete assembly of the system [6].

Table 4: Spray lengths at different injection pressures (Measured values)

S/N	Pressures (Bars)	Spray lengths (mm)
1	3	604
2	6	832
3	9	1071
4	12	1506
5	15	1785

Figures 7 to 11 shows the sprays from the produced atomizer having half spray angle of 30° at different injected pressures.

Figure 7 shows that entrainment of secondary air starts beyond 400 mm. As velocity of the spray decreases as it leaves the nozzle, the spreading of the spray becomes more pronounced because of the decrease in the velocity of the spray.

Figure 7: Spray for α = 60° and ΔP = 3 bars.

Figure 8 shows that entrainment of secondary air starts beyond 700 mm. As velocity of the spray decreases as it leaves the nozzle, the spreading of the spray becomes more pronounced because of the decrease in the velocity of the spray.

Figure 8: Spray for α = 60° and ΔP = 6 bars.

Figure 9 shows a jet which was produced when the fluid (oxygen and kerosene) was discharged through the nozzle. The spray was linear up to 600 mm because the velocity at the tip of the nozzle is more which extends until was affected by the air from the atmosphere. Beyond point 600 mm, entrainment of secondary air occurs. The free jet was produced when the fluids was discharged in the surrounding with no confinement.

Figure 9: Spray for α = 60° and ΔP = 9 bars.

The spray as observed in Figure 10 shows that entrainment of secondary air starts around 700 mm; before this point, the spray was seen to be linear because the velocity of the spray was greater at that region. The entrainment of the surrounding in the jet increases the mass of the jet but decreases the velocity of the jet as it sprays.

Figure 10: Spray for α = 60° and ΔP = 12 bars.

The entrainment of the surrounding as observed (beyond 900 mm) in Figure 11 was due to increase in mass of jet which depends on the difference in the momentum flux within the jet and that of the surrounding (note that as the jet was discharged into a still surrounding, the surrounding was set in motion). The entrainment of the surrounding will continue as long as the difference in the momentum flux exists.

Figure 11: Spray for α = 60° and ΔP = 15 bars.

Figures 12 to 16 shows the flames from the produced atomizer having half spray angle of 30° for different injected pressures.

Table 5: Flame lengths at different pressures (Measured values)

S/N	Pressures (Bars)	Flame lengths (mm)
1	3	903
2	6	1102
3	9	1401
4	12	1608
5	15	1804

The free unconfined jet spreads in the surrounding and the entrainment of the secondary air occurred around 400 mm as observed in Figure 12. The spreading of the flame was due to entrainment of the surrounding. The free jet has no confinement and hence can spread till the difference between the momentum flux (mass of the jet * velocity of the jet) of the jet and the surrounding becomes zero. Entrainment of surrounding depends on mass flow rate and jet velocity.

Figure 12: Flame for α = 60° and ΔP = 3 bars.

Due to entrainment of the surrounding as observed in Figure 13, the axial velocity of the jet decreases making the flame to start spreading beyond 600 mm. Because of the increased velocity of the jet, the flame as seen in the Figure was linear without any interference from the surrounding air.

Figure 13: Flame for α = 60° and ΔP = 6 bars.

In Figure 14, the characteristic feature of the flame as it spreads was due to the difference in the density of the jet and the surrounding. A hot jet in a cold surrounding spreads faster than a cold jet in the same surrounding. Spreading of the flame which started to occur beyond 1200 mm was due to entrainment of the surrounding.

Figure 14: Flame for α = 60° and ΔP = 9 bars.

Figure 15 shows that the flame starts spreading as a result of the surrounding air beyond point 1300 mm.

Figure 15: Flame for α = 60° and ΔP = 12 bars.

Figure 16 shows that the spreading of the hot flame as a result of the surrounding air started beyond point 1500 mm. It was

observed that there was a whitish flame formed very close to the tip of the atomizer; the flame was at the region where the velocity of the jet is high without entrainment of the secondary air. The whitish flame indicates that there was complete combustion process of the fuel.

Figure 16: Flame for $\alpha = 60°$ and $\Delta P = 15$ bars.

The graph in Figure 17 was gotten from the regression analysis of the two sample items, the injection pressure and the spray lengths. After the calculations, a relationship between the pressures and the spray lengths was established, thus the graph. The equation of best fitting line that described all the points was established and the straight line graph was plotted. At any point on y or x axis the other corresponding values can be obtained from the other axis. It was also proven that the two sample items (the pressure and spray length or flame length as the case may be) has a linear relationship that exists between them.

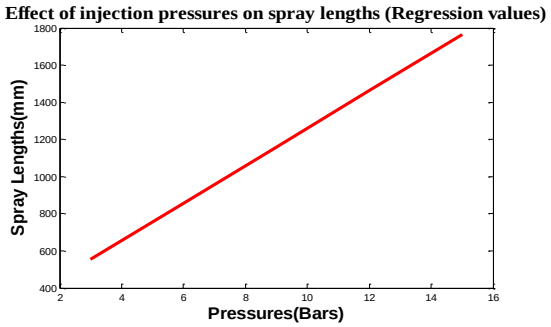

Figure 17: Effect of injected pressures on spray lengths.

The graph in Figure 18 was gotten from the regression analysis of the two sample items, the injection pressure and the flame lengths. After the calculations, a relationship between the pressures and the flame lengths was established, thus the graph. The equation of best fitting line that described all the points was established and the straight line graph was plotted. At any point on y or x axis the other corresponding values can be obtained from the other axis. It was also proven that the two sample items (the pressure and flame length) has a linear relationship that exists between them.

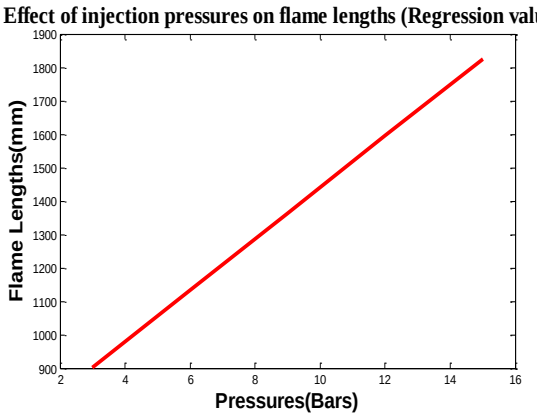

Figure 18: Effect of injected pressures on flame lengths.

Figure 19 is the graph of measured spray lengths versus injected pressures and regression values of spray lengths versus injected pressures plotted to compare how close the points (measured spray lengths and regression values of spray lengths) are. The graph of injection pressures versus the regression values of spray lengths is a linear graph but that is not the case of the graph for injection pressures versus the measured spray values; the discrepancies in the profile of the measured spray lengths was from errors while taking the readings.

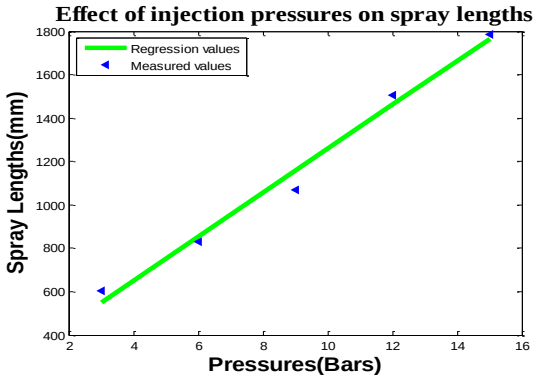

Figure 19: Effect of injected pressures on spray lengths (measured and regression values).

Figure 20 is the graph of measured flame lengths versus injected pressures and regression values of flame lengths versus injected pressures plotted to compare how close the points (measured flame lengths and regression values of flame lengths) are. From the graph it can be deduced that the readings gotten for the measured flame lengths and the corresponding regression values of flame lengths are almost the same. The error margin can be said to be negligible.

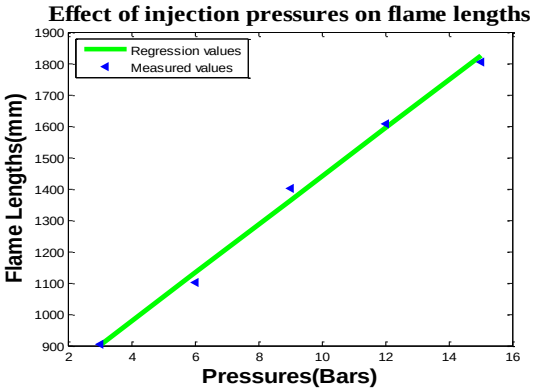

Figure 20: Effect of injected pressures on flame lengths (measured and regression values).

Table 6: Time taken to melt metals [6]

DESCRIPTIONS			
Materials	**Quantity (kg)**	**Time taken to melt material (seconds)**	**Volume of kerosene used (litres)**
Aluminum	0.6	823	0.5
Brass	1.2	1,033	1.0

4. CONCLUSION

The design of the air-blast atomizer was carried out for maximum injection pressure of 15 bars. The experiments of volumetric flow rate, spray lengths, and flame lengths were carried out with the injection pressure ranging from 3 to 15 bars. Experiments showed that at 3 bars, the spray and flame lengths are small and also that at 3 bars; liquid film was not breaking into small droplets. As injection pressure increases from 6 to 12 bars, spray lengths and flame lengths increases due to breaking of liquid film into small droplets. The effect of entrainment of the surrounding air was more at high pressures. The design and construction of this air-blast atomizer like any other atomizer fabricated locally requires little data and is very easy to construct. The atomizer produced the desired result for which it was designed for, in melting the selected metals. It can be concluded that the air-blast atomizer produced can be used for both surface and pit furnaces using kerosene as fuel [6].

5. REFERENCES

[1] Lefebvre, A. H. 1980. Air-blast Atomization: Prog. Energy science, vol. 6, pp 233 – 261.

[2] M. J. Madu, I. S. Aji, B. Martins 2014. Design, Construction and Testing of a Burner that uses an admixture of used engine oil and Kerosene for foundry application. International Journal of Innovative Research in Science, Engineering and Technology, vol. 3, issue 9.

[3] Robert Aftel 1996. Effect of atomization gas properties on droplet atomization in an air-assist atomizer. MSc. Thesis at Virginia Polytechnic Institute and State University, Virginia.

[4] Lefebvre, A. H., and Ballal, D. R. Gas Turbine Combustion 2010. Alternative Fuels and Emissions, third edition. CRC Press.

[5] Nigerian National Petroleum Corporation (NNPC) 2007. Warri Refining and Petrochemical Company Ltd, Technical Report, 4:87.

[6] Benneth Ifenna Okoli 2016. Design and Performance Evaluation of an Air-blast Atomizer, MSc. Thesis, Department of Mechanical Engineering, Lagos State University, Lagos, Nigeria.

[7] Vasiliov, A.P., Koderaftsov, B.M., Korbatinkov, B.D., Ablintsky, A.M., Polyayov, B.M. Palvian, B.Y. 1993. Principles of Theory and Calculations of Liquid Fuel Jet, Moscow.

[8] V. A. Borodin, Yu. F. Dityakin, L. A. Klyachko, V. I. Yayodkin 1967. Atomization of liquids, Foreign Technology Division.

[9] Bayvel, L. 1993. Liquid Atomization. Hemisphere Publishing Corporation, Taylor & Francis.

[10] Witold Perkowski, Andrzej Irzycki, Krzysztof Snopkiewicz Lukasz Grudzien, and Michal Kawalec 2011. Study on kerosene atomization process under high speed air stream. Journal of Kones Power train and Transport, vol. 18, no 4.

[11] Pipatpong Watanawanyoo, Sumpun Chaitep and Hiroyuki Hirahara 2009. Development of an air assisted fuel atomizer (liquid siphon type) for a continuous combustor. American Journal of Applied Sciences 6 (3): 380-386.

International Journal of Science and Engineering Applications
Volume 6–Issue 12, 372-381, 2017, ISSN:-2319–7560

Efficient Chromatic and Residual Dispersion Postcompensation for Coherent Optical OFDM

Ishiwu I. Jude
Department of Electrical/Electronics Engineering
Modibbo Adama University of Technology, Yola
Adamawa State, Nigeria

Yahya Adamu
Department of Electrical/Electronics Engineering
Modibbo Adama University of Technology, Yola
Adamawa State, Nigeria

Oguche D. Onoja
Department of Electrical/Electronics Engineering
Modibbo Adama University of Technology, Yola
Adamawa State, Nigeria

Boyson Andrew
Department of Electrical/Electronics Engineering
Modibbo Adama University of Technology, Yola
Adamawa State, Nigeria

Abstract: In lieu of other impairments associated with fiber communication such as; fiber nonlinearity, fading, Intersymbol Interference (ISI), Intercarrier Interference (ICI), Chromatic Dispersion (CD) is compensated by Coherent Optical Orthogonal Frequency Division Multiplexing (CO-OFDM) technique. This technique divides the available bandwidth into five subbands, each modulated at a low data rate and postcompensated for the Chromatic Dispersion. Implementation of the Optical OFDM involves the use of Digital Signal Processing (DSP); Inverse Discrete Fourier Transform (IDFT) and Discrete Fourier Transform (DFT) both at the transmitter and receiver respectively. The Residual Dispersion left after CD is compensated by Constellation Adjustment Method (CAM). Simulation results using Optisystem show 107-Gb/s single-channel transmission over 1000-km Standard Single Mode Fiber (SSMF) with polarization division multiplexing Four Quadrature Amplitude Multiplexing (4-QAM) using 128 DFT, 82 subcarriers, 5 pilot subcarriers and 16 guard intervals. Equally, the simulation analysis were done at various transmission distances, OFDM systems show a better Min. BER and Max. Q factor than the conventional Non-Return to Zero (NRZ) systems.

Keywords: BER, Chromatic Dispersion, CO-OFDM, Cyclic Prefix, DFT, Residual Dispersion.

1. INTRODUCTION

Orthogonal Frequency Division Multiplexing (OFDM) is a multicarrier transmission technique, which divides the available spectrum into many carriers, each one being modulated by a low rate data stream. OFDM is similar to Frequency Division Multiplexing Access (FDMA) in that the multiple user access is achieved by subdividing the available bandwidth into multiple channels, which are then allocated to users [1]. However, OFDM uses the spectrum much more efficiently by spacing the channels much closer together. This is achieved by making all the carriers orthogonal to one another, preventing interference between the closely spaced carriers.

OFDM is a widely used and very attractive modulation and multiplexing technique for broadband wireless and wired communication system due to its spectrum efficiency and channel robustness . OFDM belongs to a broader class of Multi-Carrier Modulation (MCM) carrying data over many lower rate subcarriers[2]. OFDM, forms the basis of many of several telecommunications standards in the world, counting from Digital Terrestrial Television (DTT), Wireless Local Area Networks (LANs), digital radio broadcasting and 4G mobile communications [3]. OFDM is also the source of nearly all Digital Subscribers Line (DSL) standards, and within this context, OFDM is generally known as Discrete Multi-Tone (DMT) because of some minor peculiarities.

Though, OFDM offer tremendous benefits and its wide-spread use in wireless communications, it has been considered for optical communications during the last years [4]. The need to develop a high-speed and robust communication services and the tremendous expansion of the Internet are driving the development of high-capacity and flexible optical transport networks. In recent times, many researches started to pay more interest to apply the OFDM technique with MCM, instead of Single Carrier Modulation (SCM) in optical fiber communication due to its ability to reduce the effect of selective fading, chromatic dispersion, Inter-Symbol Interference (ISI) and Inter-Carrier Interference (ICI).

Optical OFDM has gained much interest in recent years as it is developed for long-haul transmission network or rather longer distance transmission and has capability to equalize Chromatic Dispersion (CD) and Polarization Mode Dispersion (PMD) efficiently. OFDM technique has been applied so it can be utilized in Wavelength Division Multiplexing (WDM) system [5]. To attain a high spectral efficiency and achieve simple channel equalization, OFDM takes benefit of the Fast Fourier Transform (FFT) [6, 7]. Optical OFDM has become one of the most capable technologies that are used for designing bit rate and bandwidth variable transponders for spectral efficient optical networks. O-OFDM with phase modulation and coherent detection is also the future for suitable spectral efficient key, robust against system nonlinearities, and for transmission in elastic networks[8, 9].

2. THEORY

2.1 Historical Background of OFDM

Chang in 1966, first introduced the concept of OFDM in a seminal paper, he proposed a method to synthesize band limited signals for multi channel transmission. The idea is to transmit signals simultaneously through a linear band limited channel without Inter Carrier Interference (ICI) and Inter Symbol Interference (ISI) [1]. Based on Chang`s work, Salzberg in 1967, performed the analysis and came up with conclusion that the focus to design a multi channel transmission must concentrate on reducing crosstalk between adjacent channels rather than on perfecting the individual

signals. In fact, "OFDM" first appeared in his separate patent in 1970 [10].

The proposal to create the orthogonal signals using an FFT came in 1969 [11]. In 1980, the cyclic prefix (CP) was proposed [12]. For practical wireless applications, OFDM began to be considered in the mid 1980s. A paper on OFDM for mobile communications is published by Cimini of Bell Labs in 1985 [3]. In 1987, the use of OFDM for radio broadcasting is considered and the significance of combining Forward Error Correction (FEC) with OFDM is also noted by Lassalle and Alard [13]. Table 1 shows some of the key milestones of the OFDM technique in radio frequency (RF) domain.

Table 1. Historical Development of RF OFDM

S/No	Date	Author(s)	Contributions
1	1966	R. Chang	Foundation work on OFDM
2	1967	Salzberg	Performed the analysis based on Chang`s work
3	1969	S.B. Weinstein and P.M Ebert	FFT implementation of OFDM
4	1980	R.Peled and A. Ruiz	Cyclic prefix was proposed
5	1985	L. Cimini	OFDM for mobile communications
6	1987	Alard	Combination of FEC and OFDM
7	1995	ETSI	DSL formally adopted DMT, a variation of OFDM
8	1995 (1997)	ETSI	European Telecommunications Standards Institute (ETSI) Digital Audio (Video) Broadcasting standard, DAB(DVB)
9	1999 (2002)	IEEE Standard	Wireless LAN standard, 802.11 a (g), Wi-Fi
10	2004 (2007)	IEEE WiMax Forum	Wireless MAN standard, 802.16, WiMax
11	2009 (2015)	3GPP/ESTI	Long Term Evolution (LTE), 4 G mobile standard

Although, OFDM has been studied in RF domain for over four to five decades, the research on OFDM in optical communication began only in the late 1990s by the two pioneers; Pan and Green. In the late 2000s, long-haul transmission by optical OFDM has been investigated by a few groups. Two major research directions appeared, Direct Detection Optical OFDM (DDO-OFDM) looking into a simple realization based on low-cost optical components and Coherent Optical OFDM (CO-OFDM) aimed to achieve high spectral efficiency and receiver sensitivity, though with inherent complex circuit design due to digital signal processing. Since then, the interest in optical OFDM has increased dramatically. In 2007, the world's first CO-OFDM experiment with line rate of 8-Gb/s was reported [14]. In the last few years, the transmission capacity continued to grow tremendously about ten times per year. In 2009, up to 1 Tb/s optical OFDM was successfully demonstrated [15]. Table 1 shows the progress of optical OFDM in the last two decades.

Table 2. Progress of Optical OFDM

S/No	Date	Author(s)	Contributions
1	1996	Pan and Green	OFDM for Community Access Television
2	2001 2001	You and Kahn Dixon et al.,	OFDM in DD System OFDM over Multimode Fiber
3	2005 2005	Jolley et al., Lowery and Armstrong	Experiment of 10Gb/s O-OFDM over Multimode Fiber Power-efficient O-OFDM in DD Systems
4	2008	Djordjevic and Vasic Shieh and Athaudage	Long-haul transmission DDO-OFDM Long-haul transmission CO-OFDM
5	2010	Shieh et al.,	8-Gb/s CO-OFDM transmission over 1,000 km
6	2014	Yang et al	56Gb/s and 1100-Gb/s per single channel CO-OFDM using OBM
7	2016	Ma et al.,	8x520-Gb/s Signal Based on Signal Band/λ PDM-16QAM on 75-GHz Grid.
8	2017	Dar et al.,	Chromatic dispersion compensation techniques and characterization of fiber Bragg grating for dispersion compensation

Besides offline DSP, from 2009 onward, a few research groups started to investigate real-time optical OFDM transmission. The first real-time optical OFDM demonstration took place in 2009; three years later, then real-time single-carrier coherent optical reception was

demonstrated. The pace of real-time OFDM development is fast, with the net rate crossing 10-Gb/s within one year. Moreover, by using Orthogonal-Band-Multiplexing (OBM), which is a key advantage for OFDM, up to 56-Gb/s and 110-Gb/s over 600-km Standard Single Mode Fibre (SSMF) was successfully demonstrated. Recently, in 2016 another breakthrough was made, the transmission of 8x520-Gb/s Signal Based on Signal Band/λ Pulse Density Modulation (PDM)-16QAM-OFDM on a 75-GHz Grid [16]. As evidenced by the commercialization of single-carrier coherent optical receivers, it is foreseeable that real-time optical OFDM transmission with much higher net rate will materialize in the near future based on state-of-the-art Application Scientific Integrated Circuits (ASIC) design.

2.2 Optical Fibre Communications

The communication system of fibre optics is well understood by studying the parts and sections of it. The major elements of an optical fibre communication system are shown in Figure 1.

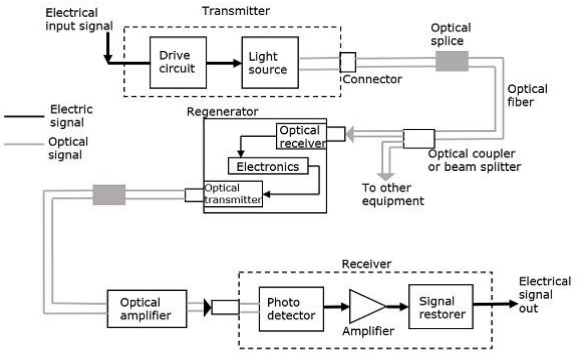

Figure 1. Block Diagram of Optical Fibre Communication System.

The basic components are light signal transmitter, the optical fibre, and the photo detecting receiver. The additional elements such as fibre and cable splicers and connectors, regenerators, beam splitters, and optical amplifiers are employed to improve the performance of the communication system.

2.3 Principle of orthogonality

Orthogonality is a property which allows multiple signals to be perfectly transmitted over a common channel and detected at the receiver without interference. Below are the three cases where frequency orthogonolality is achieved.

CASE 1: From Figure 2 below, the symbol of each OFDM has a duration, $T_s = N/R$. Expressing the OFDM signal in the time domain $S_k(t)$ as the summation of each information symbol $X_{i\,k}$ being carried in the *k*th subcarrier within the *i*th OFDM symbol. On the choice of modulation used for the subcarriers, complex values are resulted by superposition of the subcarriers, although not accounted yet on this research. The period of the OFDM symbol becomes;

$$S_k(t) = R\,\{\sum_{i=-\infty}^{\infty}.\sum_{k=0}^{N-1} X_{i,k}\, e^{j2\pi fkt}.\ P(t\text{-}iTs)\} \qquad 1$$

Where; $P(t)$ represent an ideal square pulse of length,

N, represent the number of subcarrier

while; F_k, represent the subcarrier frequency.

In equation 1 , the OFDM symbol is ideally multiplied by a square pulse $P(t)$, which is one for a T_s -second period and zero otherwise. The amplitude spectrum of that square pulse has a form $\sin(c\pi ft)$, which has zeros for all frequencies f that are an integral multiple of $1/T_s$.

CASE 2: Consider a subcarrier frequency of the equation below;

$$F_k = K\frac{1}{Ts} \qquad 2$$

We can deduce from the above equation that each subcarrier must be separated from its neighbours by exactly $1/T_s$, so each subcarrier within an OFDM symbol has exactly an integer number of cycles in the interval T_s, and the number of cycles differs by exactly one, as depicted in Figure 2. This way, orthogonality between subcarriers is achieved.

CASE 3: Consider another scenario where orthogonality is achieved, this property can be explained for any couple of subcarriers by the following expression:

$$\int_{-\frac{T}{2}}^{\frac{T}{2}} \cos(\frac{2\pi mt}{T})\ \cos(\frac{2\pi nt}{T})\ dt=0,\ m\neq 0 \qquad 3$$

We consider a situation where m & n are different natural numbers, the area under this product over one period is zero as this can be shown in Figure 2.9 for a three subcarriers. The frequencies of these waves are called harmonics and for these, the orthogonality condition is always fulfilled.

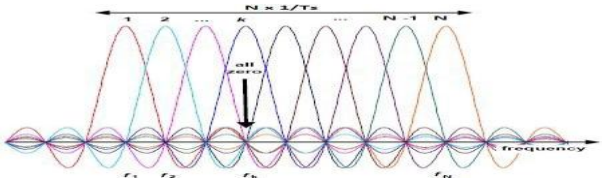

Figure 2. Time Domain Subcarriers within an OFDM symbol

2.4 Chromatic Dispersion (CP)and Equalization

Chromatic dispersion is a deterministic distortion given by the design of the optical fibre. It leads to a frequency dependence on the rate at which the phase of the wave propagates in space (optical phase velocity) and its effect on the transmitted optical signal basically scales quadratically with the data rate [17].

This frequency dependence of the phase can be easily identified by describing a pulse propagating through a monomode optical fibre in the frequency domain:

$$X_{out}(\omega) = X_{in}(\omega).e^{j\beta(\omega)z} \qquad 4$$

Where $X_{in}(\omega)$ represents the Fourier transform of the transmitted signal, $X_{out}(\omega)$ is the Fourier transform of the received signal and $ß(\omega)$ corresponds to the phase constant of the fundamental propagating mode.

Because of the frequency dependence on ß, the main limiting effect considered in equation 4 will be chromatic

dispersion. Other phenomena such as losses or nonlinearities will be not considered, though their effects in fibre propagation can be added afterwards. The consideration of dispersion as the main limiting effect in an optical transmission has been shown to be a good approach in a broad variety of practical applications, but more importantly allows the simplification of its study.

In an ideal case, the phase constant in equation 4 has a linear dependency with frequency, meaning that all the spectral components undergo the same phase delay, which is the same as saying that they travel at the same velocity. At reception the same signal will be obtained without any distortion but with a constant delay. On the other hand, in a dispersive channel the phase constant $e^{j\beta(\omega)z}$ in equation 4, has a nonlinear dependency with frequency and as a consequence of the different arrival times of the frequency components, the recovered signal at the reception end will differ from the transmitted one

In order to obtain an OFDM signal without errors at the receiver, the use of cyclic prefix is essential. This will eliminate ISI when a temporal dispersion affects the channel. However, the effect of chromatic dispersion causes the information symbols to still be affected by amplitude and phase changes when arriving to the receiver, as shown in Figure 3 below.

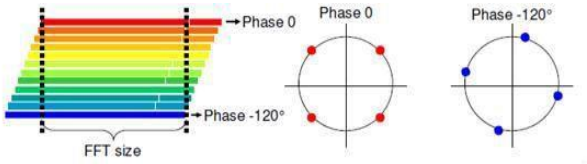

Figure 3. Phase Distortions on the Received Constellation.

Consequently, an N-level equalizing stage has to be introduced right after the FFT operation at the receiver in order to correct the phase and amplitude levels, where N is the number of received subcarriers. The design parameters for this stage should be obtained through a channel estimation, which is usually performed with training sequences. These sequences are added by using pilot subcarriers in each OFDM symbol, so the channel transfer function can be approximated. As the design of training sequences is beyond the scope of this work, the required phase compensation for each OFDM symbol will be calculated based on the dispersion model suffered by each subcarrier:

$$\varphi = \frac{1}{2} B_2 W^2 L \qquad 5$$

Where L is the fibre length, W is the subcarrier frequency, and B is the second term order of the signal phase delay approximation.

However, this equalization will be not enough to obtain the ideal received constellation, as a constant phase shift will still affect the received symbols due to the choice of the reference frequency for the fibre. Hence, the Constellation Adjustment Method proposed in this thesis will eliminate the residual chromatic dispersion left after equalization.

2.5 Coherent Optical OFDM Systems (CO-OFDM) Systems

CO-OFDM represents the ultimate performance in receiver sensitivity, spectral efficiency, and robustness against polarization dispersion, but yet requires the highest complexity in transceiver design. In the open literature, CO-OFDM was first proposed by Shieh et al., and equally formalized the concept of the coherent optical MIMO-OFDM. They carried out an early CO-OFDM experiments over 1,000 km SSMF transmission at 8-Gb/s [14]. Kaneda et al., proposed a field demonstration of 100-Gb/s real-time coherent optical OFDM detection [8].

The conceptual diagram of CO-OFDM system is shown in Figure 4 [18]. It contains five essential functional blocks: 1) RF-OFDM signal transmitter, 2) RF to optical (RTO) up-converter, 3) Optical fibre links, 4) optical to RF (OTR) down-converter, 5) RF-OFDM receiver. Such setup can be also used for single-carrier scheme, in which the DSP part in the transmitter and receiver needs to be modified, while all the other hardware setup remains the same.

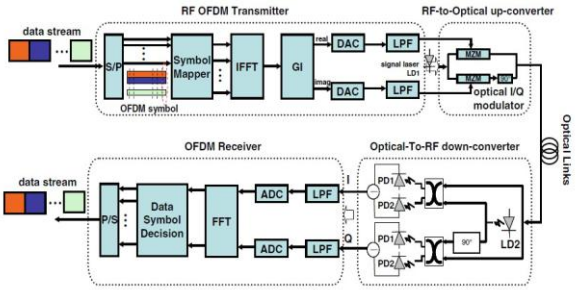

Figure 4. Block diagram of a Coherent Optical OFDM System.

When the modulation technique of OFDM combines with coherent detection, the benefit brought by these two powerful techniques are multifold: (1) High spectral efficiency; (2) Robust to chromatic dispersion and polarization-mode dispersion; (3) High receiver sensitivity; (4) Dispersion Compensation Modules (DCM)-free operation; (5) Less DSP complexity; (6) Less oversampling factor; (7) More flexibility in spectral shaping and matched filtering.

3. System Setup

The optical transmission link with and without equalizer compensation by using single channel CO-OFDM system is setup using an OptiSystem as a simulation tool. It has been used by many researchers to simulate the fibre nonlinearity and dispersion effects in optical communication systems. Simulation setting takes most key optical communication system/component parameters into account including fibre nonlinearity, noise, dispersion, etc. A generic CO-OFDM system includes five basic functional blocks as already shown and fully explained in Figure 4: OFDM transmitter, RF to Optical (RTO) up-converter, optical link, Optical to RF (OTR) down-converter, and OFDM receiver. The general parameters used for this simulation are shown in Table 3 below, while Table 4 and 5 show the Transmitter/Receiver Parameters, Optical Fibre Link Parameters and Receiver Parameters respectively;

Table 3. Simulation Parameters

S/No	Parameters	Values	Units
1	Bit rate	10e9	bit/sec
2	Time window	12.8e-9	Sec
3	Sample rate	640e9	Hz
4	Sequence length	128	Bits
5	Samples per bit	64	
6	Symbol rate	10e9	Symbols/sec
7	Sensitivity	-100	dB
8	Resolution	0.1	Nm
9	Interpolation offset	0.5	Nm
10	Number of leading zeros`	3	

Table 4. Transmitter/Receiver Parameters

S/No	Parameter	Value	Units
1	QAM Bits Per Symbol (b/sym)	2	bits
2	QAM Gray Code	No	
3	QAM Differential Coding	No	
4	OFDM Size	144	
5	OFDM Maximum possible subcarriers	128	
6	OFDM Guard interval	16	
7	OFDM used subcarrier	82	
9	OFDM unused subcarrier	41	
10	OFDM Pilot subcarrier	5	
11	Average OFDM power	12	dBm
13	CW Laser frequency	193.1	THz
14	CW Laser power	10	dBm
15	CW Laser linewidth	0.1	MHz
16	CW Laser Azimuth	45	degree
17	LPBF Cut-off frequency	0.75 x Symbol rate	Hz

S/No	Parameter	Value	units
1	Optical fibre length	100 to 1000	km
2	Attenuation	0.2	dB/km
3	Dispersion	16.75	Ps/nm/km
4	Effective area	80	μm^2
5	Reference wavelength	1550	nm
6	Optical gain	20	dB
7	Optical noise figure	4	dB
8	Ideal Dispersion Compensation FBG Bandwidth	125	GHz
9	Dispersion	-800	Ps/nm

Table 5. Optical Fibre Link Parameters

3.1 Coherent Optical-OFDM Transmitter

At the transmitter side, both modulation and multiplexing are achieved digitally using an Inverse Fast Fourier Transform (IFFT). The subcarrier frequencies are mathematically orthogonal over one OFDM symbol period. Figure 5 shows the simulation set-up for the 4-QAM CO-OFDM Transmitter. The 107-Gb/s CO-OFDM signal is generated by multiplexing five OFDM sub-bands. In each band, 21.4-Gb/s OFDM signals are transmitted in both polarizations. The QAM CO-OFDM transmitter has a gain and bias of 0.021 volt and 1.5 volt respectively. The optical frequency source is a Continuous Wave (CW) laser of 1550 nm and 10 dBm optical frequency and power respectively. The transmitted signal is generated off-line by a Pseudo-Random Bit Sequence (PRBS) Generator with $10e^9$ bits/secs and mapped to 4-QAM constellation. The digital time domain signal is formed after IFFT operation. The FFT size of OFDM is 128 carriers, and guard interval is 1/8 of the symbol window. The middle 82 subcarriers out of 128 are filled, from which five pilot subcarriers are used for phase estimation.

A Tektronix Arbitrary Waveform Generator (AWG) is used to generate analogue signals for both optical I and Q parts. The optical I/Q modulator comprising two MZMs with 90^0 phase shift is used to directly impress the baseband OFDM signal. The modulator is biased at null point to suppress the optical carrier completely and perform linear baseband-to-optical up-conversion. The signal is then propagated through the optical link and becomes degraded due to fibre impairments.

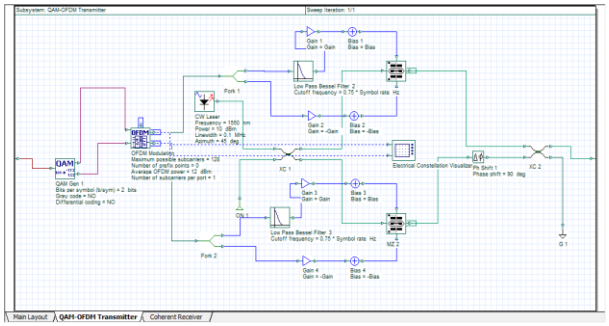

Figure 5. Architecture of 4-QAM CO-OFDM Transmitter Subsystem

3.2 Optical Fibre Link

The Fibre Link for CO-OFDM set-up consists of 100 km span of Standard Single Mode Fibre (S-SMF) including an Ideal Dispersion Compensation Fibre Bragg Grating and Optical Amplifier prior to each span. Figure 6 shows the configuration of the fibre link. The Optical Amplifier increases the link distance, which is limited by fibre loss in an optical communication system. The length of fibre can be increased by increasing the number of loops. The amplifiers have a 4-dB noise figure and a 20-dB gain, while the Optical Fibre has a dispersion of 16.75 ps/nm/km, an effective area of 80 μm^2, attenuation of 0.2-dB/km and reference wavelength of 1550 nm. The ideal dispersion compensation Fibre Bragg Gratings (FBGs) have a frequency of 193.1 THz, bandwidth of 125 GHz, dispersion of -800 ps/nm and a noise threshold of about -100 dB.

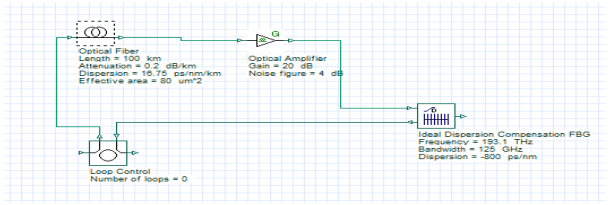

Figure 6. Architecture of CO-OFDM Fibre Link

3.3 Coherent Optical-OFDM Receiver

At the receiver side, a coherent optical receiver comprising a polarization beam splitter, a local laser, two optical 90^0 hybrids, and four balanced photo-receivers is used to down-convert the data to the RF domain. Figure 7 shows the schematic of Coherent Optical-OFDM receiver.

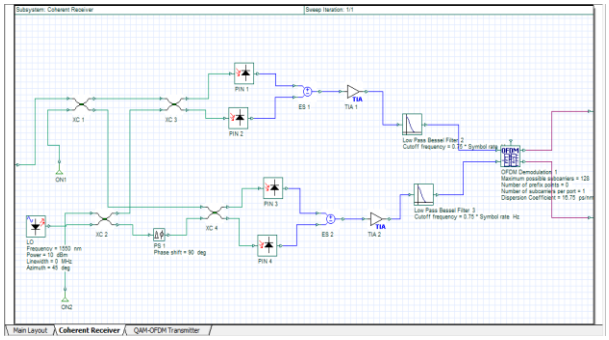

Figure 7. Architecture of Coherent Optical-OFDM Receiver Subsystem.

Finally, the complete architecture of the proposed 107-Gbps 4-QAM CO-OFDM Dispersion Compensation Post Compensated System is shown in Figure 8. However, the input data for the OFDM modulator can have different modulation formats such as BPSK, QPSK, QAM, etc.

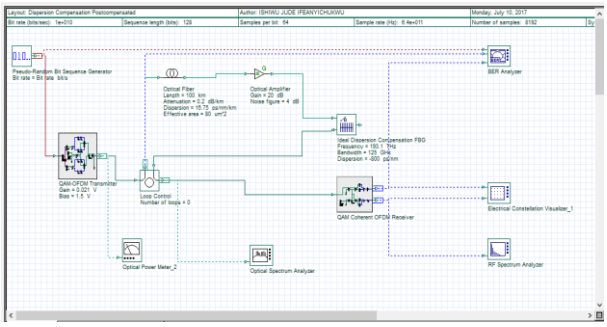

Figure 8. 107-Gb/s 4-QAM CO-OFDM Dispersion Compensation Post Compensated System.

3.4 The Logical Model

The addition of Cyclic Prefix (CP) is done immediately after Digital Signal Processing (DSP) of the Inverse Discrete Fourier Transform (IDFT) at the transmitter and removed after Analogue-to-Digital (ADC) Conversion process at the receiver. The use of cyclic prefix has been a good technique proposed by many authors in mitigating the effect of chromatic dispersion and nonlinearity in fibre-wireless base system. Although, there are some residual dispersion left after chromatic dispersion, these will be mitigated with the use of constellation adjustment method.

However, there is an effect of phase and frequency errors in terms of relationship between the time variation of phase and its effect on the received constellation. However, how these errors are corrected in the digital domain is our concern. First, we consider the case where there is no noise or distortion in the channel and *Qd = 0*, so that there is no I/Q phase imbalance. Now, from the basic theory of OFDM as earlier explained in Sec II, we were made to understand that, OFDM consists of multiple subcarriers that are orthogonal to each other. Henceforth, we deduced that the transmitted baseband OFDM signal is given as;

$$x(k) = \sum_n . \sum_{m=0}^{N-1} X_{m,n} b(m\text{-}nN_{sym}) . \exp\left(\frac{-j2\pi k_m}{N}\right) \quad 6$$

where; N is the IFFT size, $X_{m,n}$ is the m-th subcarrier data symbol transmitted on the n-th symbol, N_{sym} is the number of samples in a symbol, and $b(m)$ is the pulse shape of the m-th sample.

We equally deduced that, at the receiver side, the incoming signal $y(t)$ passing through channel can be given as;

$$y(t) = x(t) * c(t) + \eta(t) \quad 7$$

where; $c(t)$ is the impulse response of the channel, [*] is the convolution and $\eta(t)$ is the noise component of the received signal.

Using the formulae for sums and products of angle and with simple manipulation, the time domain received signal samples are given as; Θ_0

$y_m = x_m \, exp\ (j\Theta_m)$ 8

where; Θ_m is the phase error at the receiver for the *mth* sample of the OFDM symbol under consideration. For the case where there is constant phase error, $\Theta_m = \Theta_0$.

Then; $y_m = x_m \, exp\ (j\Theta_0)$ 9

And it is simple to show that;

$y_k = exp\ (j\Theta_m)\ X_k$ 10

The constellation is simply rotated by angle Θ_0 as illustrated in Figure 9 below. In an OFDM system, this would be automatically corrected in the single tap equalizer.

However, let consider the opposite extreme where the phase noise is zero mean and there is no correlation between phase noise samples E{ $\Theta_m \ \Theta_n$ } = 0, m ≠ n, where; E { } denotes the expectation operator. Then taking the FFT gives;

$$y_k = \frac{1}{\sqrt{N}} \sum_{m=0}^{N-1} y_m exp\ (\frac{-j2\pi k_m}{N}) \quad 11$$

$$y_k = \frac{1}{\sqrt{N}} \sum_{m=0}^{N-1} x_m exp(j\Theta_m) exp\ (\frac{-j2\pi k_m}{N}) \quad 12$$

If the phase error is small, then applying the small angle approximation $exp(j\Theta_m) \approx 1 + j\Theta_m$.

$$y_k = \frac{1}{\sqrt{N}} \sum_{m=0}^{N-1} x_m exp(1 + j\Theta_m) exp\ (\frac{-j2\pi k_m}{N}) \quad 13$$

$$y_k = X_k + \frac{1}{\sqrt{N}} \sum_{m=0}^{N-1} x_m exp(j\Theta_m) exp\ (\frac{-j2\pi k_m}{N}) \quad 14$$

$y_k = X_k + N_k$ 15

The demodulated subcarrier y_k is equal to the transmitted subcarrier plus a noise like term, N_k which depends on all of the transmitted subcarriers. The power of N_k can be calculated by using the fact that Θ_m and x_m are statistically independent.

3.5 Constellation Adjustment Method (CAM)

Constellation adjustment method also known as phase rotation is a method of tackling some residual dispersion left after chromatic dispersion and equalization. The steps are outlined below;

Step 1. Rotate the phase dispersion $\Theta_{(k)}$ for all the subcarriers.

Step 2. Divide the constellation points into quadrants according to the subcarrier modulation format.

Step 3. For each quadrant, calculate the centre of the points, the difference between the phase/amplitude and the theoretical constellation positions.

Step 4. For each quadrant, make adjustment to all subcarriers, to compensate the phase/amplitude discrepancies.

Figure 9 (a) shows one of the Chromatic Dispersion compensated subcarrier, where the phases are compensated by $\Theta_{(k)}$. The residual rotation is still visible in Figure 9 (b). This is compensated as well by the constellation adjustment, as shown in Figure 9 (c). Figure 9 (d) shows the constellation of all compensated subcarriers.

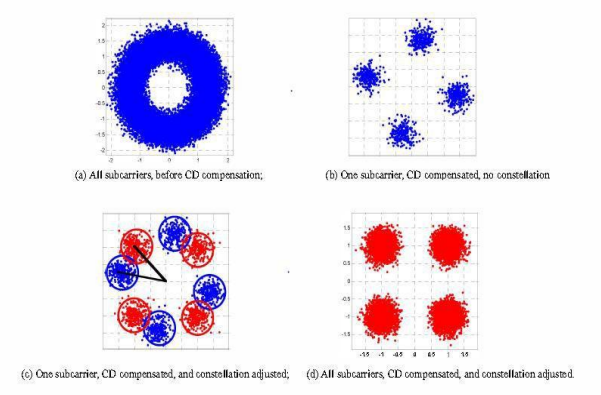

Figure 9. Constellation Adjustment for Phase Rotations.

The algorithm for the proposed residual chromatic dispersion compensation is shown in Figure 10 below. It is a smoothing algorithm, that shows sequences in realizing the proposed post compensation dispersion compensation, constellation adjustment method.

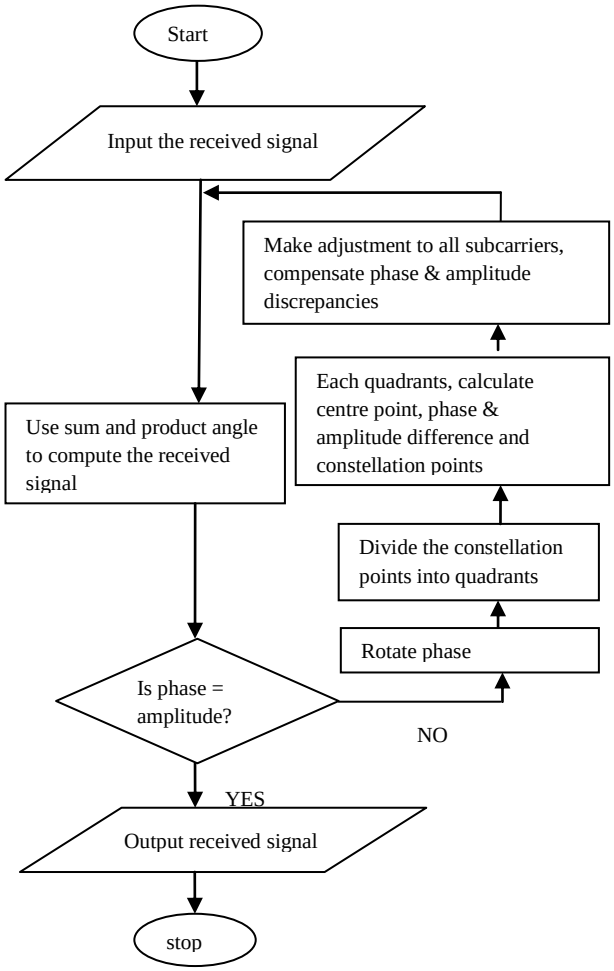

Figure 10. Algorithm for the Compensation of Residual Dispersion

4. RESULTS AND DISCUSSIONS

4.1 Simulation Results for the Proposed System.

The performance evaluation of the proposed system was done using OptiSystem. A single channel of 4-QAM CO-OFDM with a data rate of 107-Gb/s was simulated over various transmission distances (n loops), Optical Signal to Noise Ratio (OSNR) and number of subbands. Note that any change in the fibre physical parameters will distort the form of the received constellation. The OFDM symbol size of 144, which consists of a DFT size of 128 with a guard interval of 16 and a data sample of 82 subcarriers, which consists 5 pilot subcarriers and 41 unused subcarriers were used for the simulation.

Once the simulation is executed, the OptiSystem Analyzer tools will display the optical power by Optical Power Meter, received optical spectrum and RF spectrum by Optical Spectrum and RF Spectrum Analyzers respectively. While the received constellation diagrams are displaced by Electrical Constellation Visualizers and finally, its corresponding Bit Error Rate (BER) by BER Analyzer. Figure 11 shows the received optical power displayed after 4-QAM CO-OFDM Transmitter, while Figure 12 and Figure 13 show the received optical spectrum plotted after fibre link and received RF spectrum plotted after radio link respectively. Figure 14 and Figure 15 show the received 4-QAM CO-OFDM constellation before CD and after CD respectively. Finally, Figure 16 shows the BER value displayed by the BER Eye Diagram.

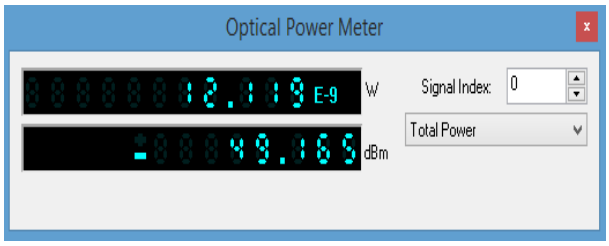

Figure 11. Received Optical Power after 4-QAM CO-OFDM Transmitter.

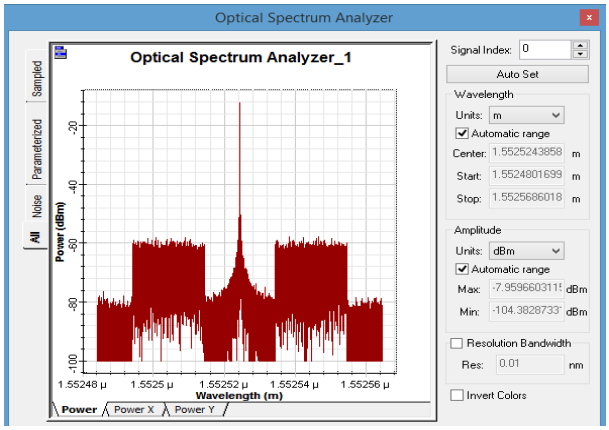

Figure 12. Received Optical Spectrum after Fibre Link

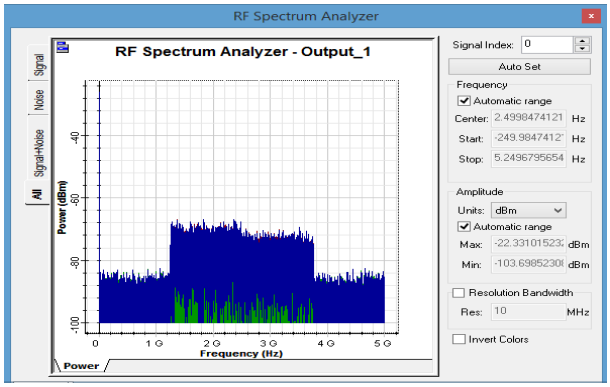

Figure 13. Received Radio Frequency Spectrum after Radio Link

The 4-QAM COFDM constellation shown in Figure 14 resembled a doughnut shape, this is due to non addition of cyclic prefix in the transmission. Consequently, the inter symbol interference, inter carrier interference and other impairments associated with fiber lead to poor quality signal. However, with addition of cyclic prefix, Figure 15 is obtained after equalization and employing the proposed technique; combination of CO-OFDM technique with Constellation Adjustment Method post compensated. A far better signal quality is realized as compared to Non-Return-Zero system.

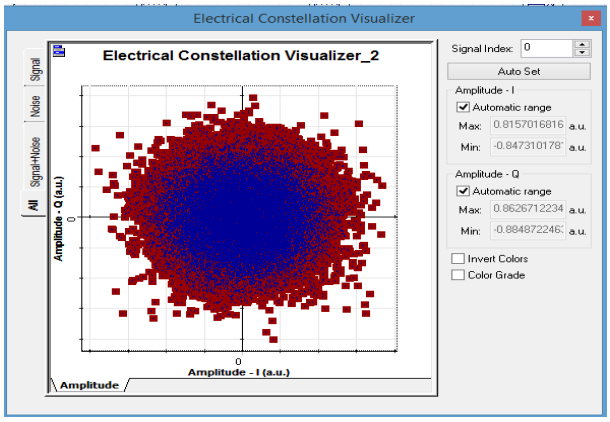

Figure 14. Received Optical Constellations for 4-QAM CO-OFDM before CD.

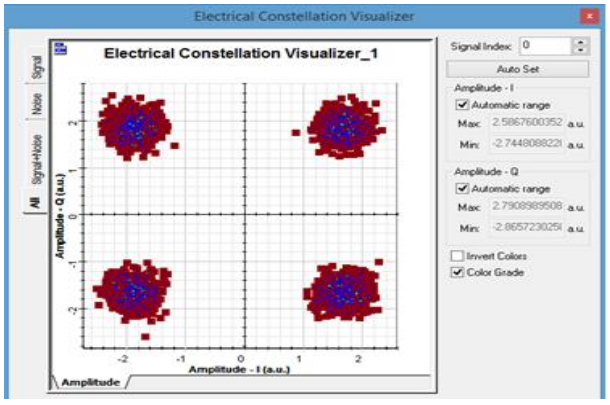

Figure 15. Received Optical Constellations for 4-QAM CO-OFDM after CD.

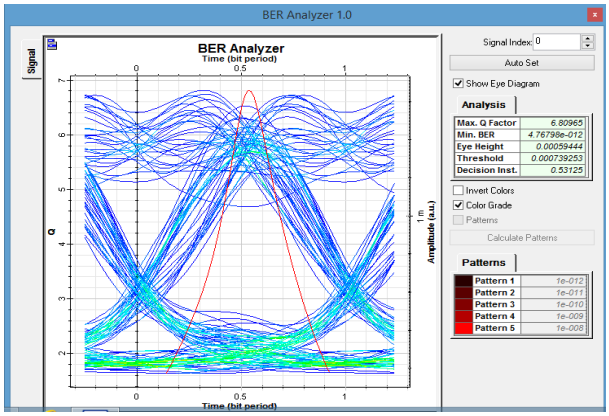

Figure 16. BER Eye Diagram for 4-QAM CO-OFDM Post Compensation.

The BERs of NRZ, 4 QAM-OFDM, 4 PSK-OFDM systems against the same OSNR was estimated. The proposed 4-QAM CO-OFDM and 4-PSK CO-OFDM systems use a 10 GHz brick-wall optical filter before the coherent receivers, while the NRZ system uses a 20 GHz brick-wall optical filter. The NRZ transmitter and receiver have a zero linewidth laser and a 7.5 GHz fourth order Bessel filter respectively.

Figure 17 shows BER v/s OSNR, calculated over a bandwidth of 12.5-GHz. NRZ needs a 1-dB and 0.5-dB better OSNR than 4-QAM CO-OFDM and 4-PSK CO-OFDM for Min. BER of 4.76798e-12 and Max. Q factor of 6.80965 respectively. Hence, the proposed CO-OFDM chromatic dispersion post compensated systems outperformed or rather showed superior BER in comparison to the conventional NRZ system in the case of the same number of parameters.

In addition, phase rotation of the proposed system removed the discontinuity and compensated for the residual dispersion left after chromatic dispersion compensation. Hence, adoption of the smoothing algorithm to the estimated channel improved BER performance in the proposed system.

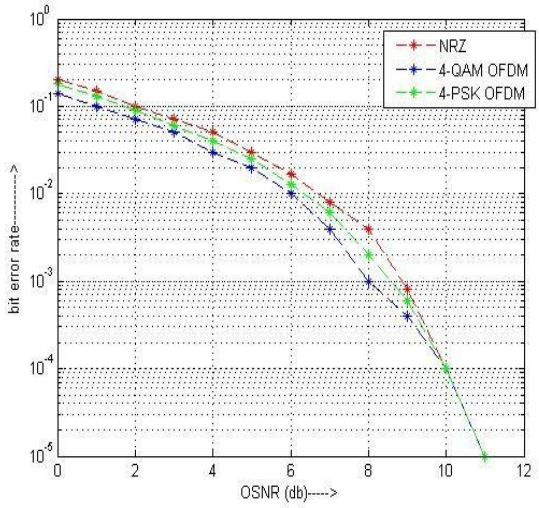

Figure 17. BER v/s OSNR for OFDM and NRZ systems.

4.2 Simulation Results at Different Loops (Distances)

The statistical analysis and results of the Min. BER and Max. Q factor for different distances after incorporating a dispersion management scheme into the coherent OFDM simulator is shown in Table 6 below. Note; in each of the loops (multiple of 100km), the simulation is done for 10 iterations and the Min. BER and Max. Q factors were recorded.

Table 6. Results of Min. BER and Max. Q Factors for Different Distances.

S/No	Distance (km)	Min. BER	Max. Q factor
1	100	4.76798e-12	6.80965
2	200	6.19523e-12	6.77137
3	300	6.30997e-12	6.76898
4	400	6.98688e-12	6.75381
5	500	7.11726e-12	6.75097
6	600	7.76709e-12	673832
7	700	8.38695e-12	6.72724
8	800	9.17197e-12	6.71401
9	900	9.40691e-12	6.71085
10	1000	1.02198e-11	6.69855

From the simulation result shown in Table 6, we can deduced that a better signal quality is gotten at a closer distance but degrades as the distance increases. This is due to transmission impairments (fading, chromatic dispersion, etc) associated with long-haul transmission network. A combination of addition of Cyclic Prefix (CP) and Constellation Adjustment Method (CAM) compensated for these impairments.

5. CONCLUSION

All the transmission impairments including higher order dispersion were compensated. To effectively and efficiently compensate for the residual dispersion, CO-OFDM combined with the Constellation Adjustment Method was proposed. The proposed implementation required no computational complexity or rather extra digital signal processing to implement. The non high frequency requirement for its operation is another added advantage to the proposed system. The simulation results showed that the proposed system theoretically achieved transmission speed of 107-Gb/s single channel CO-OFDM over 1000km optical transmission fibre.

6. ACKNOWLEDGMENTS

Our immeasurable thanks to the experts who have contributed towards development of the Optisystem Software which aided us in our simulation. More so, to the Sony Ericson Research Center and Communication Lab, Modibbo Adama University of Technology, Yola, Adamawa State, Nigeria, which provided us with the physical fiber layers for this research.

RFERENCES

[1] R. W. Chang, "Synthesis of band-limited orthogonal signals for multichannel data transmission," *Bell Systems Tech. Journal*, vol. vol. 45, pp. pp.1775–1796, 1966.

[2] S. John, E. Akinola, F. Ibikunle, C. Ndujiuba, and B. Akinaade, "Modeling of Orthogonal Frequency Division Multiplexing (OFDM) for Transmission in Broadband Wireless Communications," *Journal of Emerging Trends in Computing and Information Sciences*, vol. 3, pp. 534-539, 2012.

[3] L. J. Cimini Jr, "Analysis and simulation of a digital mobile channel using orthogonal frequency division multiplexing," *Communications, IEEE Transactions on*, vol. 33, pp. 665-675, 1985.

[4] S. B. Alexander, M. Y. Frankel, S. W. Chaddick, R. C. Litz, and C. D. Smith, "High-speed optical transponder systems," ed: Google Patents, 2015.

[5] S. Amiralizadeh, A. T. Nguyen, C. S. Park, and L. A. Rusch, "Single-Fiber Lightwave Centralized WDM-OFDMA-PON With Colorless Optical Network Units," *Journal of Optical Communications and Networking*, vol. 8, pp. 196-205, 2016.

[6] M. Chen, X. Xiao, Z. R. Huang, J. Yu, F. Li, Q. Chen, *et al.*, "Experimental demonstration of an IFFT/FFT size efficient DFT-spread OFDM for short reach optical transmission systems," *Journal of Lightwave Technology*, vol. 34, pp. 2100-2105, 2016.

[7] N. Chide, S. Deshmukh, and P. Borole, "Implementation of OFDM System using IFFT and FFT," *International Journal of Engineering Research and Applications (IJERA)*, vol. 3, pp. 2009-2014, 2013.

[8] N. Kaneda, T. Pfau, H. Zhang, J. Lee, Y.-K. Chen, C. J. Youn, *et al.*, "Field demonstration of 100-Gb/s real-time coherent optical OFDM detection," *Journal of Lightwave Technology*, vol. 33, pp. 1365-1372, 2015.

[9] E. Giacoumidis, S. Mhatli, T. Nguyen, S. T. Le, I. Aldaya, M. E. McCarthy, *et al.*, "Comparison of DSP-based nonlinear equalizers for intra-channel nonlinearity compensation in coherent optical OFDM," *Optics letters*, vol. 41, pp. 2509-2512, 2016.

[10] B. R. Salzberg, "Performance of an efficient parallel data transmission system," *Transmission Communication Technology Journal of IEEE* vol. 15, pp. 805-813, Dec, 1967.

[11] a. S. B. W. J. Salz, "Fourier transform communication system " *In Proceedings of the first ACM symposium on Problems in the optimization of data communications systems, ACM*, pp. pp. 99-128, October 1969.

[12] A. Peled and A. Ruiz, "Frequency domain data transmission using reduced computational complexity algorithms," in *Acoustics, Speech, and Signal Processing, IEEE International Conference on ICASSP'80.*, 1980, pp. 964-967.

[13] R. Lassalle and M. Alard, "Principles of modulation and channel coding for digital broadcasting for mobile receivers," *EBU Tech. Rev*, vol. 224, pp. 168-190, 1987.

[14] W. Shieh, X. Yi, and Y. Tang, "Transmission experiment of multi-gigabit coherent optical OFDM systems over 1000 km SSMF fibre," *Electronics letters*, vol. 43, p. 1, 2007.

[15] A. Sano, E. Yamada, H. Masuda, E. Yamazaki, T. Kobayashi, E. Yoshida, *et al.*, "No-guard-interval coherent optical OFDM for 100-Gb/s long-haul WDM transmission," *Journal of Lightwave Technology*, vol. 27, pp. 3705-3713, 2009.

[16] Y. Ma, Q. Yang, Y. Tang, S. Chen, and W. Shieh, "1-Tb/s single-channel coherent optical OFDM transmission with orthogonal-band multiplexing and subwavelength bandwidth access," *Lightwave Technology, Journal of*, vol. 28, pp. 308-315, 2010.

[17] D. Patel, V. K. Singh, and U. Dalal, "Assessment of fiber chromatic dispersion based on elimination of second-order harmonics in optical OFDM single sideband modulation using Mach Zehnder Modulator," *Fiber and Integrated Optics*, vol. 35, pp. 181-195, 2016.

[18] Q. Yang, Z. He, Z. Yang, S. Yu, X. Yi, and W. Shieh, "Coherent optical DFT-spread OFDM transmission using orthogonal band multiplexing," *Optics express*, vol. 20, pp. 2379-2385, 2012.